Journal of ELECTRONIC MATERIALS, Vol. 47, No. 10, 2018
https://doi.org/10.1007/s11664-018-6481-5
© 2018 The Minerals, Metals & Materials Society

Morphological Evolution and Growth Kinetics of Interfacial Cu_6Sn_5 and Cu_3Sn Layers in Low-Ag Sn-0.3Ag-0.7Cu-*x*Mn/Cu Solder Joints During Isothermal Ageing

Y. TANG,[1,3] S.M. LUO,[1] Z.H. LI,[2] C.J. HOU,[1] and G.Y. LI[2]

1.—College of Automation, Zhongkai University of Agriculture and Engineering, Guangzhou 510225, China. 2.—School of Electronic and Information Engineering, South China University of Technology, Guangzhou 510641, China. 3.—e-mail: tangyu_mycauc@163.com

The morphological evolution and growth kinetics of interfacial Cu_6Sn_5 and Cu_3Sn intermetallic compound (IMC) layers between Cu substrates and Sn-0.3Ag-0.7Cu-*x*Mn (x = 0 wt.%, 0.02 wt.%, 0.05 wt.%, 0.1 wt.%, and 0.15 wt.%) (SAC0307-*x*Mn) solders were investigated. After ageing, the uneven scallop-like morphology of Cu_6Sn_5 transforms into a layer-like morphology, and the Cu_3Sn morphology remains layer-like. Kirkendall voids at the Cu/Cu_3Sn interface and in the Cu_3Sn layer are observed at high ageing temperatures. The Cu_6Sn_5 layer predominantly governs the growth of the total IMC layer at low ageing temperatures, whereas the Cu_3Sn layer primarily influences the total IMC layer at high ageing temperatures. The growth of the Cu_6Sn_5 and Cu_3Sn layers fits a power–law relationship with an exponent between 0.44 and 0.82, indicating that IMC growth is primarily controlled by diffusion but may also be affected by interfacial reactions. The activation energies and interdiffusion coefficients of the Cu_6Sn_5 and Cu_3Sn layers were determined. The addition of Mn nanoparticles strongly affected the growth of the Cu_6Sn_5 layer but weakly impacted the growth of the Cu_3Sn layer, particularly at low ageing temperatures. Adding Mn nanoparticles to the SAC0307 solder can evidently increase the activation energy of the Cu_6Sn_5 layer, reduce the atomic diffusion rate, and inhibit the excessive growth of the Cu_6Sn_5 IMC.

Key words: Lead-free solder, Mn nanoparticles, Intermetallic compound, Growth kinetics, Activation energy

INTRODUCTION

Sn–Ag–Cu (SAC) solder is considered the best replacement for lead-based solders because of its relatively good wetting characteristics with substrates, excellent fatigue resistance, and superior joint strength in the microelectronics industry. However, some drawbacks, including the formation of a large brittle Ag_3Sn intermetallic compound (IMC) and poor drop-impact reliability, remain uncorrected.[1–3] In addition, the high cost of Ag is a main factor that limits its applications in practical use.[4] Therefore, the development of low-Ag SAC solders is urgently needed for microelectronic products. Sn-0.3Ag-0.7Cu (SAC0307) solder is a low-Ag lead-free solder in the SAC family and possesses the major advantage of forming a thin brittle Ag_3Sn intermetallic layer during the soldering process because of its low-Ag content.[5,6] Moreover, the cost of the SAC0307 solder is relatively low in the SAC family as a result of its low-Ag content.[7] However, relative to the commonly used Sn-3.0Ag-0.5Cu (SAC305), the SAC0307 solder is characterized by a high melting point, overgrowth of the interfacial IMC, and low strength, which hinder its application.[8,9]

Adding reinforcement particles to low-Ag SAC solders is considered the most effective method of

(Received October 30, 2017; accepted June 25, 2018; published online July 3, 2018)

solving the aforementioned problems.[10] Wu et al.[11] studied the formation and growth of the Cu-Sn IMC layer at the interface between low-Ag SAC0307 composite solder and Cu during ageing, and they found that the intermixing of nano-TiO_2 particles in the low-Ag SAC0307 solder joints effectively delayed the growth of the IMC layer. Kanlayasiri et al.[12] reported that the introduction of 3.0 wt.% In into SAC0307 solder can effectively lower the melting temperature by 11.5°C and suppress the growth of the Cu_3Sn layer due to reduced Cu_6Sn_5-to-Cu_3Sn conversion. Wang et al.[13] reported that the wettability of Sn-0.3Ag-0.7Cu-0.5 Ga-xPr solders can be considerably improved by adding an approximate amount of Pr. In such a case, the formation of a well-distributed $PrSn_3$ IMC can provide sites for heterogeneous nucleation, subsequently leading to the refinement of the β-Sn matrix and reduction in the growth of IMCs. Wu and Xue et al.[14] noted that adding 0.06 wt.% Pr to SAC0307 solder can improve the wettability, shear force and ductility properties. Moreover, in this example, the thickness of the interfacial IMC layer decreased to approximately 40.5% of that of the nanomodified solder joint. Gu et al.[15] reported that adding an optimal quantity of nano-Fe_2O_3 particles to Sn-1.0Ag-0.7Cu solder can suppress the formation and growth of the IMC layer at the Cu/solder interface, which the authors attributed to a decrease in free energy caused by the adsorption of nano-Fe_2O_3 particles onto the Cu surface. Leong et al.[16] reported that a small addition of Al to the Sn-1.0Ag-0.7Cu solder can reduce the thickness of the interfacial Cu_6Sn_5 IMC but has no considerable effect on the thickness of Cu_3Sn during isothermal ageing. Shnawah et al.[17] found that the addition of Mn particles to low-Ag content SAC solder joints effectively improved the thermal-cycling reliability without sacrificing drop-impact performance. Liu et al.[18] reported that Mn-doped low-Ag SAC105 alloys achieved higher drop test and dynamic bending test reliability than did SAC105 and SAC305. Lin et al.[19] found that the addition of Mn particles to Sn-1.0Ag-0.5Cu solder can dramatically suppress undercooling from the solidification of Sn because $MnSn_2$ provides heterogeneous nucleation sites for the solidification of Sn dendrites. Although the effects of reinforcement particles added to low-Ag SAC solders on the wettability, solidification, and mechanical behaviors of low-Ag SAC solder and interfacial IMC growth have been reported, the effects of Mn addition, especially nanoparticle addition, on interfacial IMC growth in low-Ag SAC0307-xMn solder joints during the isothermal ageing process have seldom been studied. Notably, in most previous related studies, the IMC was treated as a single layer, not two individual layers of Cu_6Sn_5 and Cu_3Sn, which should exhibit different growth kinetics.[5,20] The objective of the present work is to distinguish the two IMC layers from each other and investigate the effect of Mn nanoparticle addition on the individual morphological evolution and growth of the Cu_6Sn_5 and Cu_3Sn layers in low-Ag SAC0307-xMn/Cu solder joints during isothermal ageing.

EXPERIMENTAL

Composite Solder Preparation

The morphology of the SAC0307 solder, which was used as a lead-free solder in this study, is shown in Fig. 1. The SAC0307 solder particles are spherical, and their average diameter was 27.4 μm. A field-emission scanning electron microscopy (SEM) image of the Mn nanoparticles (> 99.8% purity; Nanostructured & Amorphous Materials, USA), which were used for reinforcement, is shown in Fig. 2. The Mn nanoparticles possess an irregular polygonal shape, and the average size of the Mn nanoparticles is 18 $\pm$ 3 nm in diameter. Five different compositions of the Mn-containing SAC0307-xMn (x = 0 wt.%, 0.02 wt.%, 0.05 wt.%, 0.1 wt.%, and 0.15 wt.%) composite solders were prepared by mixing different weight percentages of the Mn nanopowder into the SAC0307 solder paste in a quartz ceramic crucible. To ensure a uniform distribution of Mn nanoparticles, the mixture was mechanically blended for at least 45 min.

SAC0307-*x*Mn/Cu Solder Joint Formation

Commercial Cu strips with dimensions of 15 mm × 15 mm × 0.2 mm were used as the substrates in this work. The Cu substrates were ground with SiC papers of various grit, polished with 0.25 μm diamond paste to a mirror surface, and dipped into 50% nitric acid (HNO_3) to remove any oxide layer. To eliminate the effect of the solder volume on the experimental results, SAC0307-xMn composite solders with a weight of approximately 0.1 g were extruded from the tube through the piston rod, which was controlled by a computer, and dropped onto the Cu substrate. Subsequently, the solders and substrate were placed in an infrared reflow oven, as shown in Fig. 3. A typical reflow

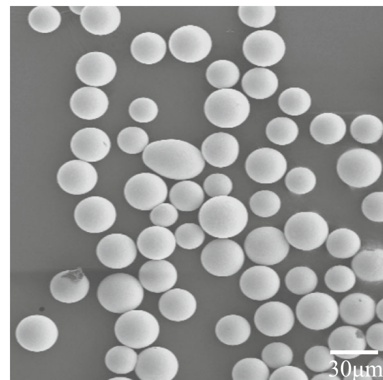

Fig. 1. SEM image of the SAC0307 solder particles.

temperature profile is shown in Fig. 4. The total reflow time was approximately 5 min, and the time above the melting temperature of 227°C (eutectic point of SAC0307) was 56 s. After the reflow soldering, the specimens were removed from the infrared reflow oven, cooled in air, cleaned with acetone to remove the residual flux, and aged in a DHG-9023A ageing oven at temperatures of 100°C, 150°C, or 190°C for 0 h, 48 h, 144 h, 288 h, 576 h, 864 h, or 1152 h.

Metallographic Preparation and Interfacial Morphology Observations

For the metallographic observations, the specimens were removed from the ageing oven, cut perpendicularly, mounted in Klarmount, ground with SiC papers of various grit, and cooled with flowing water. They were then polished with a 5-μm Al_2O_3 suspension and subsequently with 0.25 μm diamond paste. Then, the specimens were etched in a dilute solution of 2% concentrated hydrochloric acid (HCl), 6% concentrated nitric acid (HNO_3), and 92% H_2O for approximately 25 s to determine their microstructure. This process provided contrast between the IMC phases and the solder matrix. To observe the microstructure evolution of the intermetallic grains, the solders on top of the IMC were chemically dissolved using 13% (by volume) HNO_3. SEM with a voltage of 20 keV was used in backscattered mode to better discern the individual intermetallic phases. Electron-probe microanalysis (EPMA) and x-ray diffraction (XRD) were used to characterize the composition of the IMC phases. The thickness of the IMC layer was measured using Photoshop Image software. As illustrated in Fig. 5, the overall IMC layers consisted of two parts, and their thickness was calculated as follows[5]:

$$y = y_1 + y_2 \tag{1}$$

$$y_1 = \frac{\sum_{i=1}^{n} A_i}{X} \tag{2}$$

$$y_2 = \frac{S_B}{X} \tag{3}$$

where y is the total IMC layer thickness, y_1 is the Cu_6Sn_5 layer thickness, y_2 is the Cu_3Sn layer thickness, A_i is the sum of all areas of the Cu_6Sn_5 phase, S_B is the area of the Cu_3Sn layer, and X is the measured length. Twenty measurements were used to calculate the average thickness of the IMC layer after the initial reflow soldering and isothermal ageing under each set of ageing conditions.

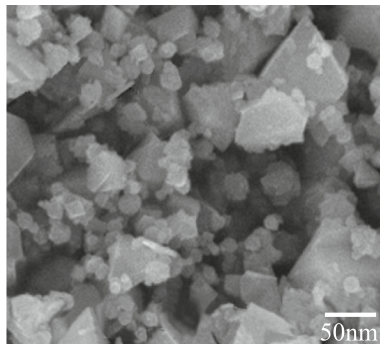

Fig. 2. Field-emission SEM image of the Mn nanoparticles.

RESULTS AND DISCUSSION

Microstructure Evolution of the Interfacial Cu_6Sn_5 and Cu_3Sn Layers

The EPMA mapping images of the SAC0307-0.15Mn solder are shown in Fig. 6. From the EPMA maps, it is clear that Mn elements are finely distributed in the SAC0307 solder and that Mn

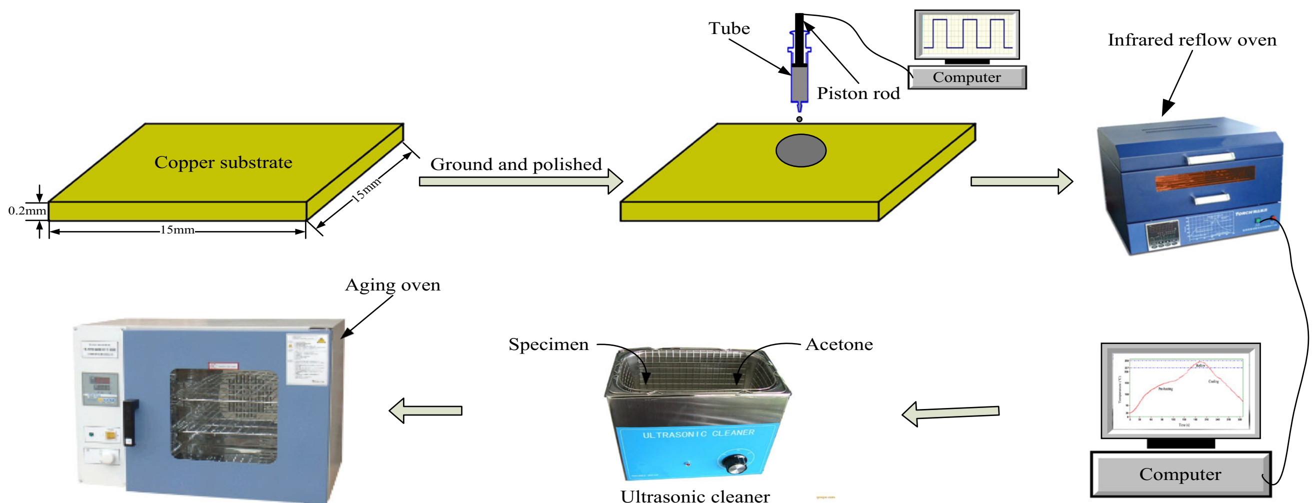

Fig. 3. Schematic of the formation of the SAC0307-*x*Mn/Cu solder joints after the reflow and ageing process.

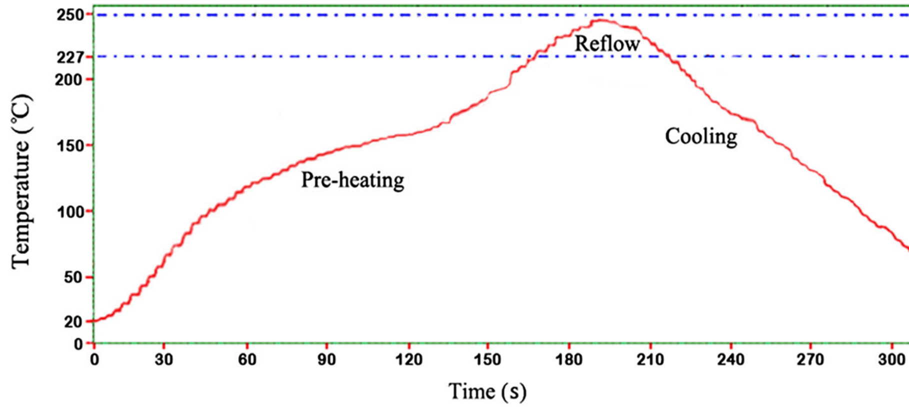

Fig. 4. Typical reflow temperature profile.

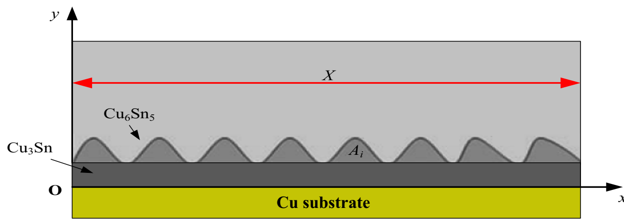

Fig. 5. Schematic of the thickness measurement of individual intermetallic layers.

nanoparticles are almost uniformly blended with the SAC0307 solder. Figures 7 and 8 show typical backscattered SEM micrographs of the cross-sectional view of the SAC0307-*x*Mn (x = 0 wt.%, 0.1 wt.%, 0.15 wt.%) solder joints, which were aged at 100°C or 190°C for 48 h or 1152 h, respectively. As evident in the figures, a duplex structure of IMCs was formed at the solder/Cu interface. The EPMA results in Fig. 7g and h show that the IMC phases were η-Cu_6Sn_5 and ε-Cu_3Sn. The layer in contact with the solder is the Cu_6Sn_5 phase, and the layer sandwiched between the Cu_6Sn_5 layer and the Cu substrate is the Cu_3Sn phase. The Cu_3Sn layer is notably thin and can be found in all five composite solder alloys. Normally, the first IMC phase that forms at the solder/Cu interface is the η-Cu_6Sn_5 phase because η-Cu_6Sn_5 has a lower activation energy than the ε-Cu_3Sn phase. The phase formation and evolution in the interfacial region involve the diffusion of Sn and Cu atoms. The formation of the Cu_6Sn_5 IMC is mainly attributed to the reaction between Cu atoms from the Cu substrate and Sn atoms from the solder, as expressed in Eq. 4.[21]

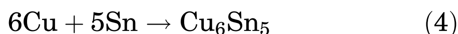

$$6Cu + 5Sn \rightarrow Cu_6Sn_5 \quad (4)$$

However, the η-Cu_6Sn_5 phase is thermodynamically unstable with Cu. Upon the formation of the η-Cu_6Sn_5 phase, the ε-Cu_3Sn phase will form by consuming the η-Cu_6Sn_5 phase, as described in Eq. 5.[21]

$$Cu_6Sn_5 + 9Cu \rightarrow 5Cu_3Sn \quad (5)$$

With a prolonged ageing time, the growth of the Cu_3Sn IMC is mainly governed by the interdiffusion between the Sn atoms through the Cu_6Sn_5 layer and the Cu atoms from the Cu substrate at the Cu/Cu_3Sn interface. This reaction is described in Eq. 6.[19]

$$3Cu + Sn \rightarrow Cu_3Sn \quad (6)$$

Moreover, the Cu_6Sn_5 layer gradually transforms from an uneven scallop-like morphology to a layer-like morphology with prolonged ageing time, and similar behavior was observed by Chiu et al.[22] This phenomenon may be the result of the shorter diffusion distance between the scallop valleys and the Cu substrate compared with the distance between the scallop peaks and the Cu substrate. Thus, Cu atoms diffuse faster to the scallop valleys than to the scallop peaks, thereby increasing the growth rate in valleys and subsequently planarizing the Cu_6Sn_5 layer. Under all the investigated conditions, the Cu_3Sn layer exhibits a layer-like and more uniform morphology than the Cu_6Sn_5 layer. Some white particles, denoted as C, were embedded in the Cu_6Sn_5 layer, as shown in Fig. 7d–f. The EPMA analysis of particle C in Fig. 7d is shown in Fig. 7i. The result reveals that particle A is the Ag_3Sn phase. Both the Cu_6Sn_5 and Cu_3Sn layers in the Mn-containing solder joints are thinner than those of the Mn-free solder joints under identical conditions. The effect of Mn nanoparticles on the individual IMC layer growth mechanism is discussed in detail in the next section.

Because of the reaction in Eq. 6, the amount of Cu atoms that diffuse from the Cu substrate to the Cu_6Sn_5/solder interface is remarkably reduced when the thickness of the Cu_3Sn layer increases with increasing ageing time. Simultaneously, the supply of Cu atoms from the solder is limited because most of the Cu atoms have been used to form Cu_6Sn_5 particles in the solder matrix, as shown in Fig. 7e. Therefore, the growth of the

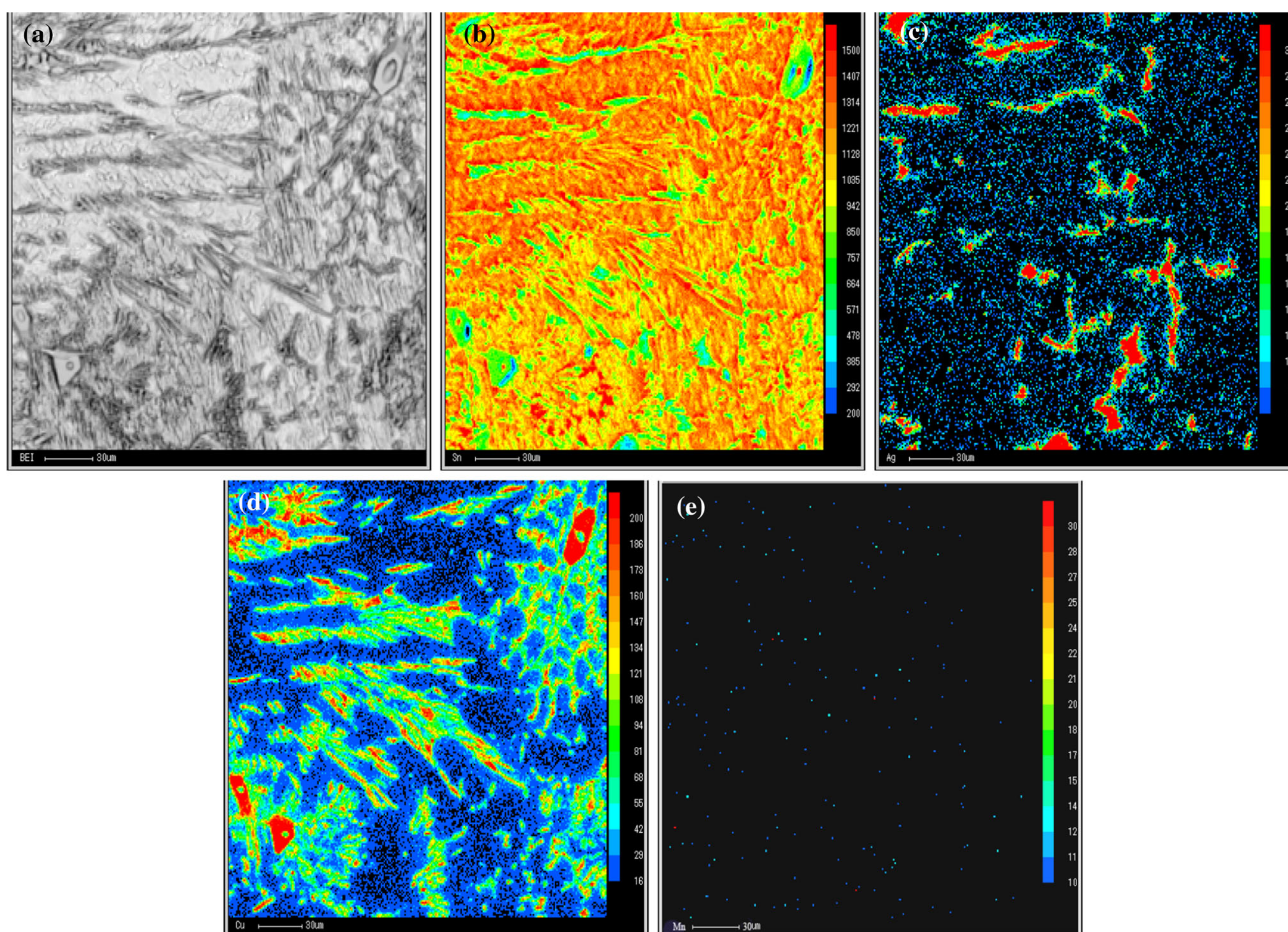

Fig. 6. EPMA mapping images of the SAC0307-0.15Mn solder: (a) SEM view, (b) Sn mapping, (c) Ag mapping, (d) Cu mapping, and (e) Mn mapping.

Cu_3Sn layer is more significant than that of the Cu_6Sn_5 layer during the ageing process. To clearly understand the growth of the Cu_3Sn layer, we measured the proportion of the Cu_3Sn layer in the total IMC layers; the results are shown in Fig. 9. At lower ageing temperatures (e.g., 100°C and 150°C), the proportion of the Cu_3Sn layer is less than 40%, which suggests that the Cu_3Sn layer is always thinner than the Cu_6Sn_5 layer in the investigated solder joints. At higher ageing temperatures (e.g., 190°C), the growth rate of the Cu_3Sn layer increases remarkably. When the ageing time is extended to 1152 h, the proportion of the Cu_3Sn layer approaches 50%, which suggests that the Cu_3Sn layer is almost as thick as the Cu_6Sn_5 layer at an ageing temperature of 190°C. Hence, the Cu_6Sn_5 layer plays a dominant role in the growth of the total IMC layer at lower ageing temperatures, whereas the Cu_3Sn layer significantly contributes to the total IMC layer at higher ageing temperatures. In addition, at a given ageing temperature, the Cu_6Sn_5 and Cu_3Sn layers simultaneously thicken with the ageing time. However, the Cu_3Sn layer exhibits a higher rate of increase in thickness than does the Cu_6Sn_5 layer. To understand the physics behind this phenomenon, the diffusion coefficients and kinetics of the Cu_6Sn_5 and Cu_3Sn layers are investigated in the next section.

Numerous microvoids formed in the Cu_3Sn layer and at the Cu/Cu_3Sn interface after the ageing process at 190°C, as shown in Fig. 8. These microvoids were not observed after ageing at 100°C, as shown in Fig. 7. These microvoids are generally referred to as Kirkendall voids.[23] Table I shows the EPMA results of the average concentration at the top and bottom of the Cu_3Sn layer in the SCA0307-xMn/Cu solder joints after ageing at 190°C for 1152 h. The Cu concentration decreased from the top to the bottom of the Cu_3Sn layer in the SCA0307-xMn/Cu solder joints. This result indicates that the Cu atoms diffuse faster than the Sn atoms in the Cu_3Sn layer during ageing. Hence, the atomic-level vacancies that remain on the substrate when the Cu atoms migrate are not filled by Sn atoms. This finding indicates that the massive diffusive flux of Cu atoms from the substrates is prominent at high temperatures. For the case of x = 0, these microvoids propagate and coalesce into

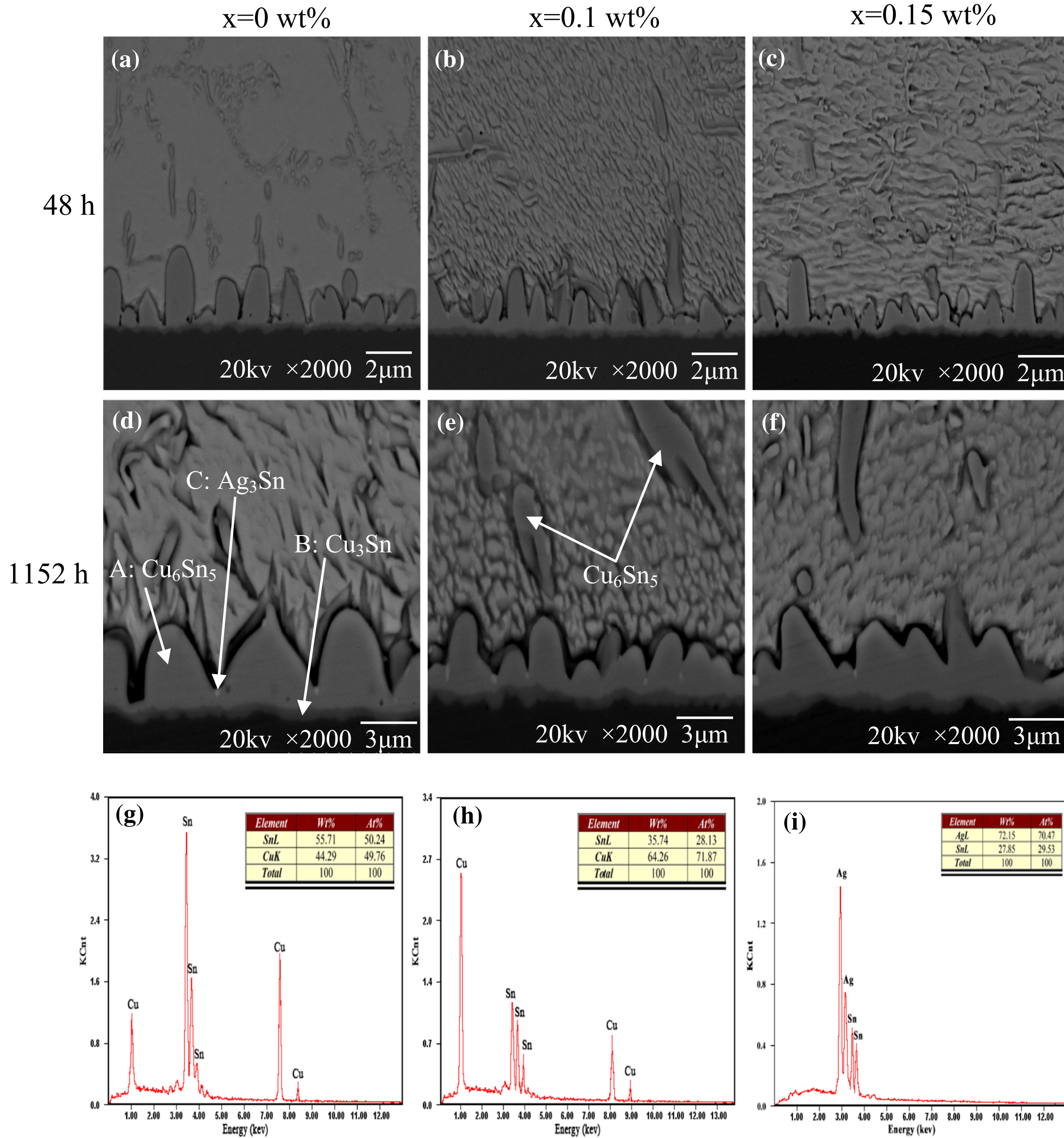

Fig. 7. Microstructure analysis of SAC0307-*x*Mn solder joints aged at 100°C for 48 h or 1152 h: (a–f) SEM micrographs, (g) EMPA analysis results for region A, (h) EMPA analysis results for region B, and (i) EMPA analysis results for region C.

a layered structure at the Cu/Cu_3Sn interface when the ageing time is increased to 1152 h, as shown in Fig. 8d. The voids at the Cu/Cu_3Sn interface show that this interphase boundary is an efficient vacancy sink in the reactive interdiffusion system. Notably, the number of Kirkendall voids substantially decreases with the addition of Mn nanoparticles, as shown in Fig. 8e and f, which is attributed to the atomic vacancies on the Cu substrate that are filled by Mn atoms.

Top Morphology of IMC Grains

Top-view SEM micrographs of three types of SAC0307-*x*Mn (x = 0 wt.%, 0.1 wt.%, and 0.15 wt.%) solder joints, which were aged at 190°C for 0 h, 144 h, and 1152 h respectively, are shown in Fig. 10. Before ageing, the Cu_6Sn_5 surface was relatively rough, many cobblestone-like grains were observed, and the gaps between the IMC grains were large, as shown in Fig. 10a–c. After 144 h of ageing, the Cu_6Sn_5 surface became flatter and exhibited an irregular polygonal type, and the grains were closely connected, as shown in Fig. 10d–f. When the ageing time approached 1152 h, the grains were significantly coarse, and some small grains merged together to become larger grains, as shown in Fig. 10h, in which the remnants of the disappearing grain boundary can clearly be observed. Hence, each large grain is formed from

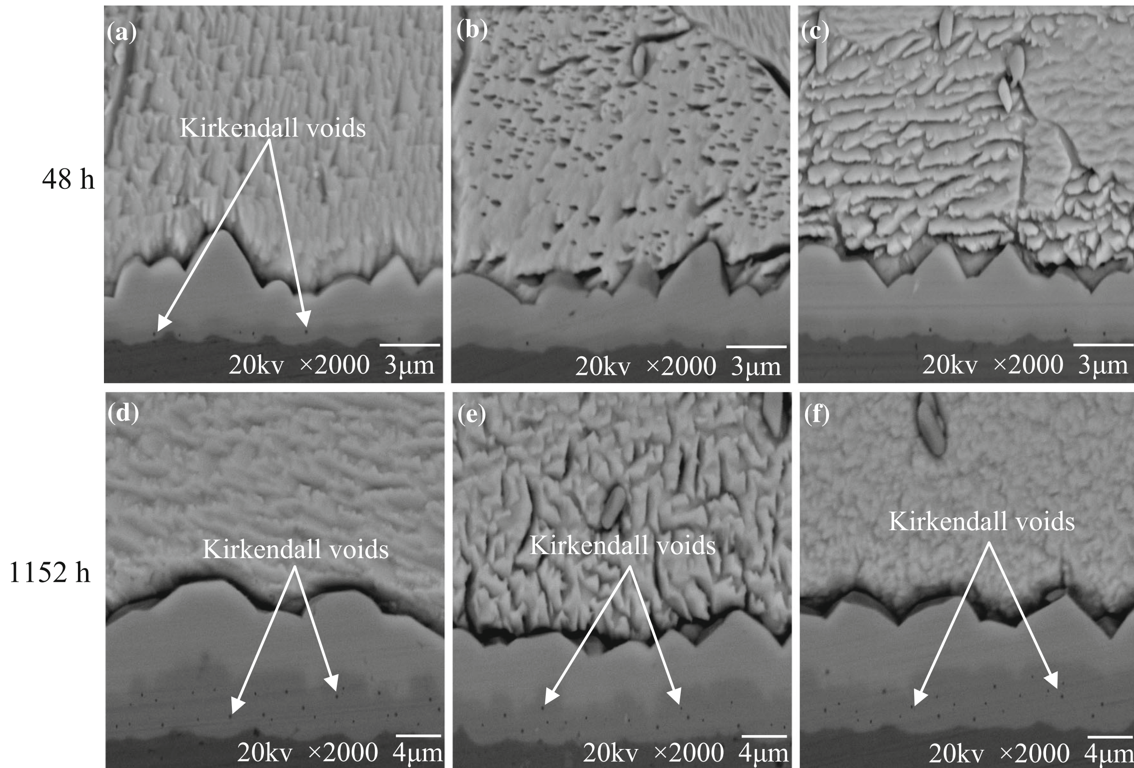

Fig. 8. SEM micrographs of the cross-sectional view of SAC0307-*x*Mn solder joints aged at 190°C for 48 h or 1152 h: (a, d) *x* = 0 wt.%, (b, e) *x* = 0.1 wt.%, and (c, f) *x* = 0.15 wt.%.

two or more small grains. In addition, the IMCs in the Mn-containing solder joint have a smaller grain size than those in the Mn-free solder joint. The grain size of the IMCs decreases with increasing Mn proportion, which may indicate that adding Mn nanoparticles helps to refine the grain size of the IMC and improve the mechanical properties of the solder joints. This conclusion is further supported by the IMC grain size distributions and standard deviations of sample measurements for different Mn nanoparticle proportions aged at 190°C for 144 h or 1152 h, as shown in Fig. 11. The results clearly reveal that the standard deviation of the grain size measurements in the Mn-free solder joints is larger than that in the Mn-containing solder joints.

Growth Kinetics of the Interfacial Cu_6Sn_5 and Cu_3Sn Layers

The growth kinetics of the IMC layer in a solid-state reaction is generally considered to follow an empirical power–law relationship[21]:

$$(y - y_0) = kt^n \tag{7}$$

where y is the average thickness of the IMC layer at time t; y_0 is the initial thickness of the IMC layer in the as-soldered joint; k is a proportional constant; t is the ageing time; and n is the growth exponent. If n is equal to 0.5, the IMC growth is controlled by diffusion; if n is equal to 1, the IMC growth is controlled by the interface reaction rate.

To study the mechanism by which Mn nanoparticles added to the SAC0307 solder inhibit the IMC layer growth in the solder joints, the Cu_6Sn_5 and Cu_3Sn layers were individually characterized, and the average thickness of the individual IMC layer was measured. Based on Eq. 7, the average thickness of the individual IMC layer versus the ageing time at different ageing temperatures is plotted in Figs. 12 and 13. The results reveal that the growth exponent n of the Cu_6Sn_5 and Cu_3Sn layers is 0.45–0.82 and 0.44–0.63, respectively. Thus, the growth exponent depends on the ageing temperature, IMC phase, and proportion of Mn nanoparticles. For the Cu_6Sn_5 and Cu_3Sn layers, a higher ageing temperature corresponds to a smaller growth exponent. At an ageing temperature of 100°C, the growth exponent of the Cu_6Sn_5 layer strongly deviates from 0.5 but is less than 0.82, which indicates that the growth of the Cu_6Sn_5 layer is not completely diffusion-controlled but is also affected by the chemical reaction. At the ageing temperatures of 150°C and 190°C, the growth exponent of the Cu_6Sn_5 layer tends towards 0.5, which indicates that the growth of the Cu_6Sn_5 layer can be controlled by diffusion. A possible explanation for this phenomenon is the increase in the size of the scallop-like grains and the morphological flattening

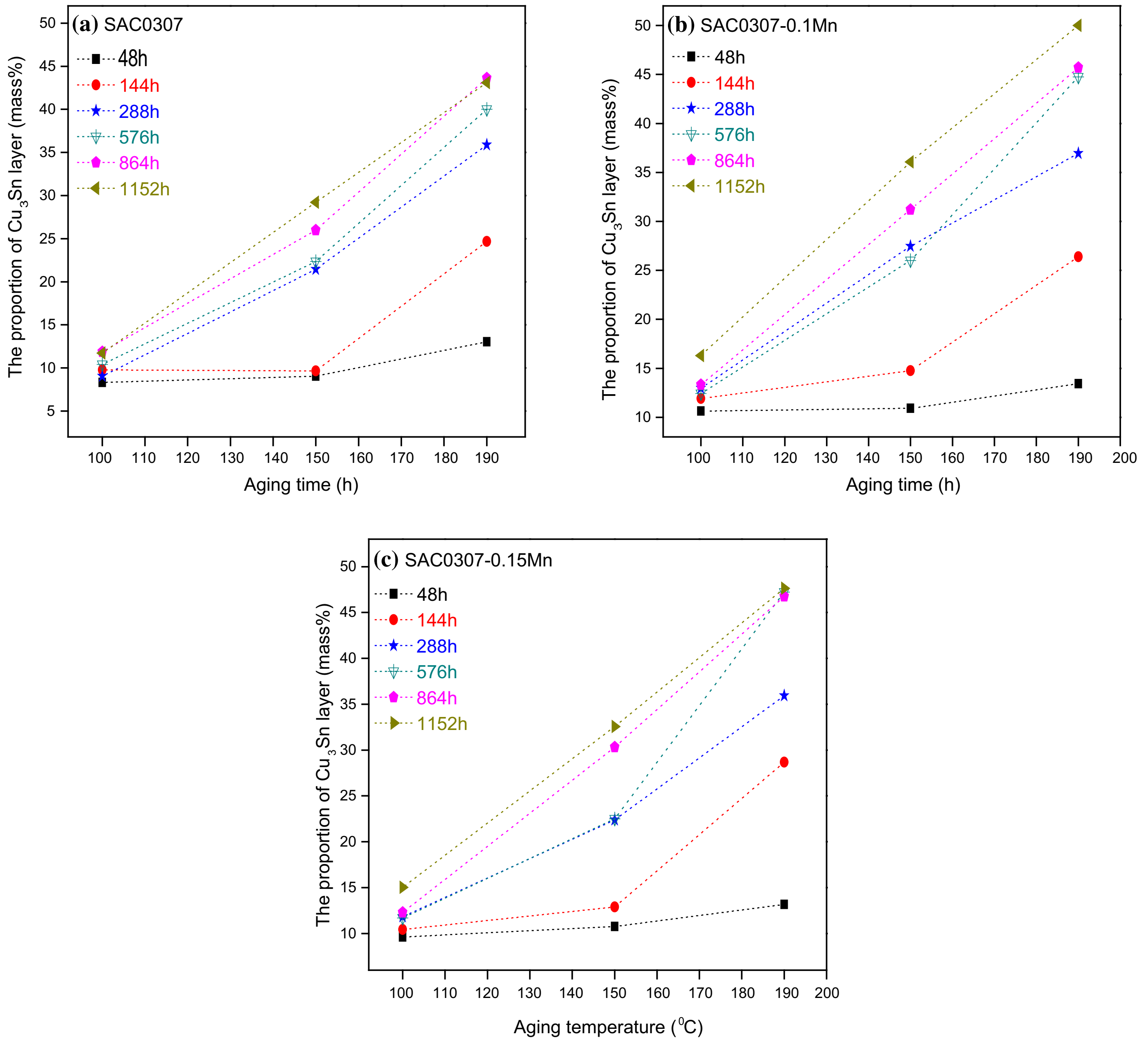

Fig. 9. Proportion of the Cu_3Sn layer in the total IMC layers for the SAC0307-*x*Mn solder joints: (a) $x = 0$ wt.%, (b) $x = 0.1$ wt.%, and (c) $x = 0.15$ wt.%.

Table I. The EPMA results of the average concentration at the top and bottom of the Cu_3Sn layer in the SCA0307-*x*Mn/Cu solder joints after ageing at 190°C for 1152 h

		Composition (wt.%)		
Solder joint	**Location**	**Cu**	**Sn**	**Mn**
SAC0307/Cu	Top	70.05	29.95	0
	Bottom	68.43	31.57	0
SAC0307-0.1Mn/Cu	Top	71.12	28.73	0.15
	Bottom	70.03	29.85	0.12
SAC0307-0.15Mn/Cu	Top	70.45	29.31	0.24
	Bottom	69.18	30.64	0.18

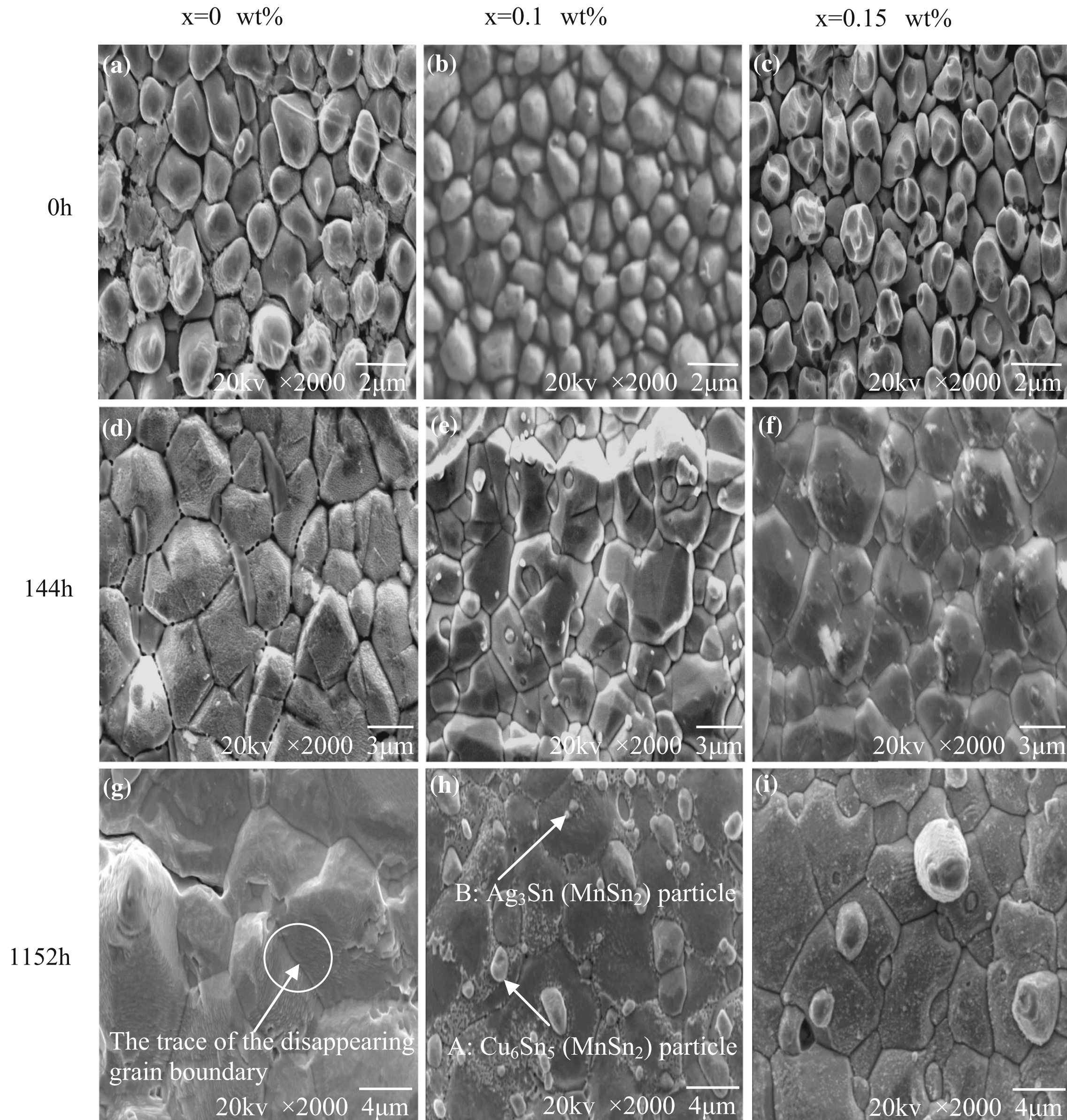

Fig. 10. Top-view SEM micrographs of the SAC0307-xMn solder joints aged at 190°C for 0 h, 144 h, and 1152 h: (a, d, g) x = 0 wt.%, (b, e, h) x = 0.1 wt.%, and (c, f, i) x = 0.15 wt.%.

with increasing ageing temperature. The narrow channels between the scallop-like grains gradually vanish, and the growth mechanism controlled by the interface reaction rate weakens. Finally, the growth of the Cu_6Sn_5 layer becomes diffusion-controlled, and the growth exponent n approaches 0.5. Notably, at three different ageing temperatures, the growth exponent of the Cu_3Sn layer is approximately 0.5, which indicates that the growth of the Cu_3Sn layer during ageing is mainly governed by the interdiffusion between the Sn atoms that diffuse through the Cu_6Sn_5 layer and the Cu atoms from the Cu substrate at the Cu/Cu_3Sn interface.

Moreover, the diffusion coefficient cannot be determined using Eq. 7. Based on the data in Table II, the average growth exponent n is approximately 0.5, which indicates that IMC growth may be mainly controlled by an interdiffusion-controlled mechanism during ageing. Hence, the diffusion coefficients of the Cu_6Sn_5 and Cu_3Sn layers can be estimated using the diffusion-controlled law[24]:

$$(X - X_0) = \sqrt{Dt} \tag{8}$$

where D is the diffusion coefficient and is a function of temperature, as expressed by the Arrhenius equation[24]:

$$D = D_0 e^{-Q/RT} \tag{9}$$

where D_0 is a temperature-independent constant known as the frequency factor, Q is the activation

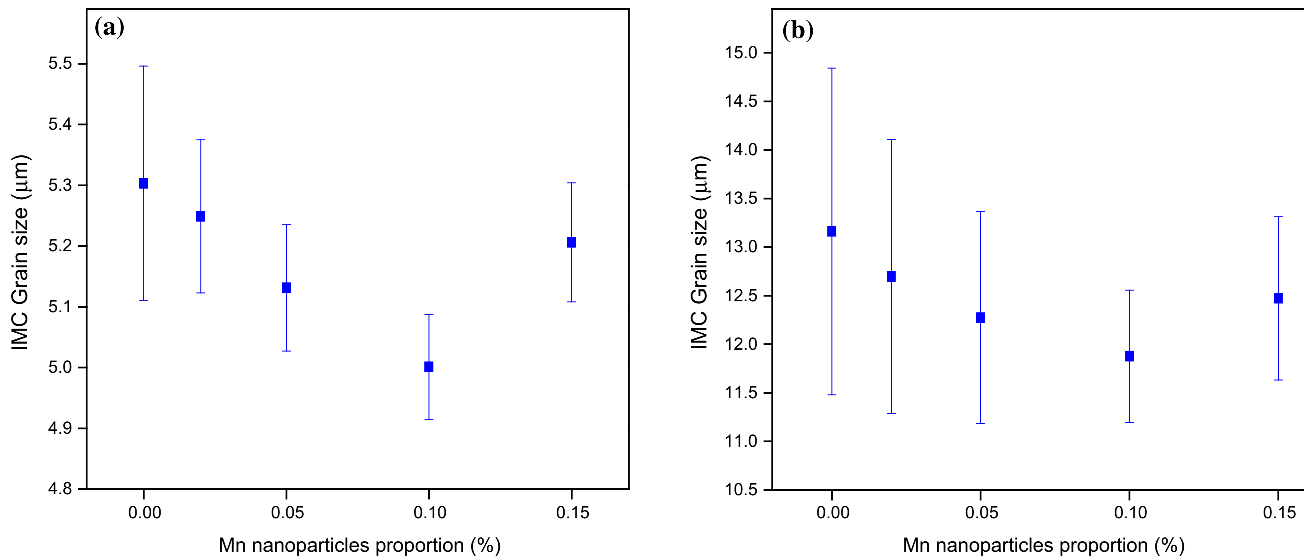

Fig. 11. IMC grain size distributions for samples with different Mn nanoparticle proportions aged at 190°C for (a) 144 h or (b) 1152 h.

energy, R is the universal gas constant, and T is the absolute temperature. When the thickness of the IMC layer ($X - X_0$) is plotted against the square root of the ageing time ($\sqrt{t}$), the slope of the graph is equal to the square root of the diffusion coefficient ($\sqrt{D}$). Figure 14 shows the diffusion coefficients of the Cu_6Sn_5 and Cu_3Sn layers at different ageing temperatures. Both the Cu_6Sn_5 and Cu_3Sn layers have higher diffusion coefficients at an ageing temperature of 190°C than at an ageing temperature of 100°C. At high ageing temperatures (e.g., 190°C), the diffusion coefficients of the Cu_3Sn layer are larger than those of the Cu_6Sn_5 layer. However, at the ageing temperature of 100°C, the diffusion coefficient of the Cu_3Sn layer is lower than that of the Cu_6Sn_5 layer. These results show that the Cu_3Sn phase contributes more to the total IMC layer growth at higher temperatures than at lower temperatures. The results also show the evident effects of the addition of Mn nanoparticles on the diffusion coefficients. For the Cu_6Sn_5 layer, with an increase in the Mn nanoparticle proportion from 0 wt.% to 0.1 wt.%, the diffusion coefficient rapidly decreases; however, further increases in the Mn nanoparticle proportion have very little influence on the diffusion coefficients at the three different ageing temperatures. For the Cu_3Sn layer, the effects of Mn nanoparticles on the diffusion coefficients of the Cu_3Sn and Cu_6Sn_5 layers exhibit identical trends at high ageing temperatures (e.g., 190°C), but, at the ageing temperature of 100°C, the diffusion coefficient of the Cu_3Sn layer remains almost unchanged at approximately 10^{-15} cm^2/s.

The activation energies of both the Cu_6Sn_5 and Cu_3Sn layers in solder joints are determined in Eq. 9 and shown in Fig. 15. The results indicate that the activation energies for the growth of the Cu_6Sn_5 and Cu_3Sn layers in different solders are 24.95–32.19 kJ/mol and 74.19–77.99 kJ/mol, respectively. The significantly lower activation energy of the Cu_6Sn_5 layer compared with that of the Cu_3Sn layer can be used to explain the earlier formation of the Cu_6Sn_5 phase during reflow. Additionally, the Mn-free solder joint has the lowest activation energy of the Cu_6Sn_5 layer. When 0.02 wt.% of Mn nanoparticles was added, the activation energy increased to 24.95 kJ/mol. The activation energy continuously increased and reached the highest value of 32.19 kJ/mol when 0.1 wt.% of Mn nanoparticles was added. However, a further increase in the Mn nanoparticle proportion to 0.15 wt.% resulted in a decrease in the activation energy to 28.82 kJ/mol. Moreover, the activation energies of Cu_3Sn do not significantly change with changes in the Mn nanoparticle proportion and range from 74.19 kJ/mol to 77.99 kJ/mol when 0.1 wt.% of Mn nanoparticles is added.

Effect of Mn Nanoparticles on the Growth of Individual IMC Layers

From the above discussion, the results of the diffusion coefficients and activation energies show that the addition of Mn nanoparticles (up to 0.1 wt.%) can effectively reduce the growth rate of Cu_6Sn_5 at three different ageing temperatures. However, it has less effect on the Cu_3Sn layer growth, particularly at low ageing temperatures. The top view of SAC0307-*x*Mn solder joints aged at 190°C for 144 h or 1152 h in Fig. 10d–i shows that many fine particles are pinned along the grain boundary of the Cu_6Sn_5 layer in the specimens both with and without Mn nanoparticles, but the densities of the particles are different. The EPMA analyses of fine particles A and B in Fig. 10h are shown in Figs. 16 and 17, respectively. The results reveal that the composition of particle A is

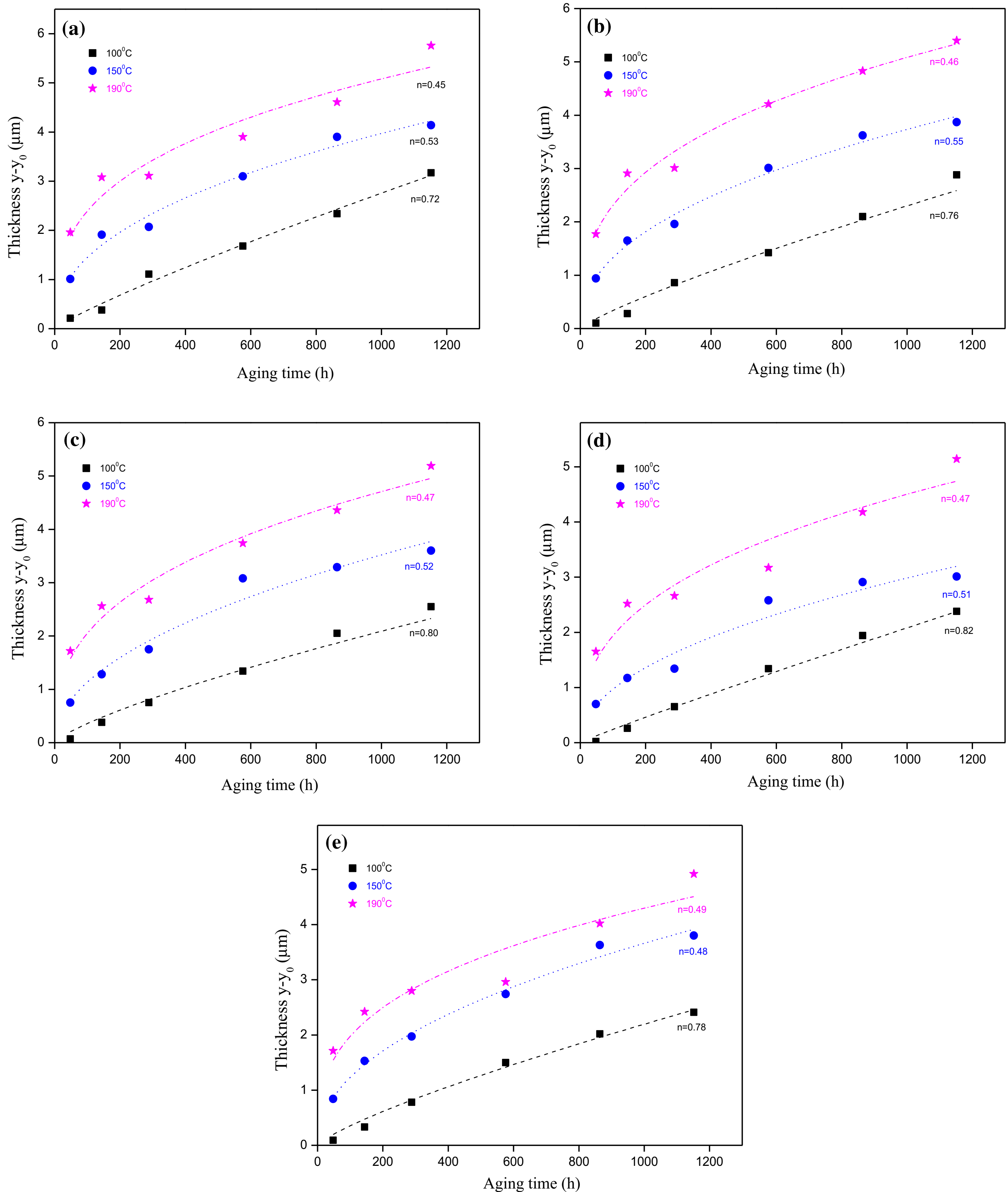

Fig. 12. Thickness of the Cu_6Sn_5 IMC layer versus ageing time for SAC0307-*x*Mn solder joints with different Mn nanoparticle proportions: (a) x = 0 wt.%, (b) x = 0.02 wt.%, (c) x = 0.05 wt.%, (d) x = 0.1 wt.%, and (e) x = 0.15 wt.%.

47.76 wt.% Sn, 51.28 wt.% Cu, and 0.96 wt.% Mn and that the composition of particle B is 30.12 wt.% Sn, 69.37 wt.% Ag, and 0.51 aw% Mn. To further confirm the phases of particles A and B, XRD analysis was performed, as shown in Fig. 18. The results further suggest that particle A consists of

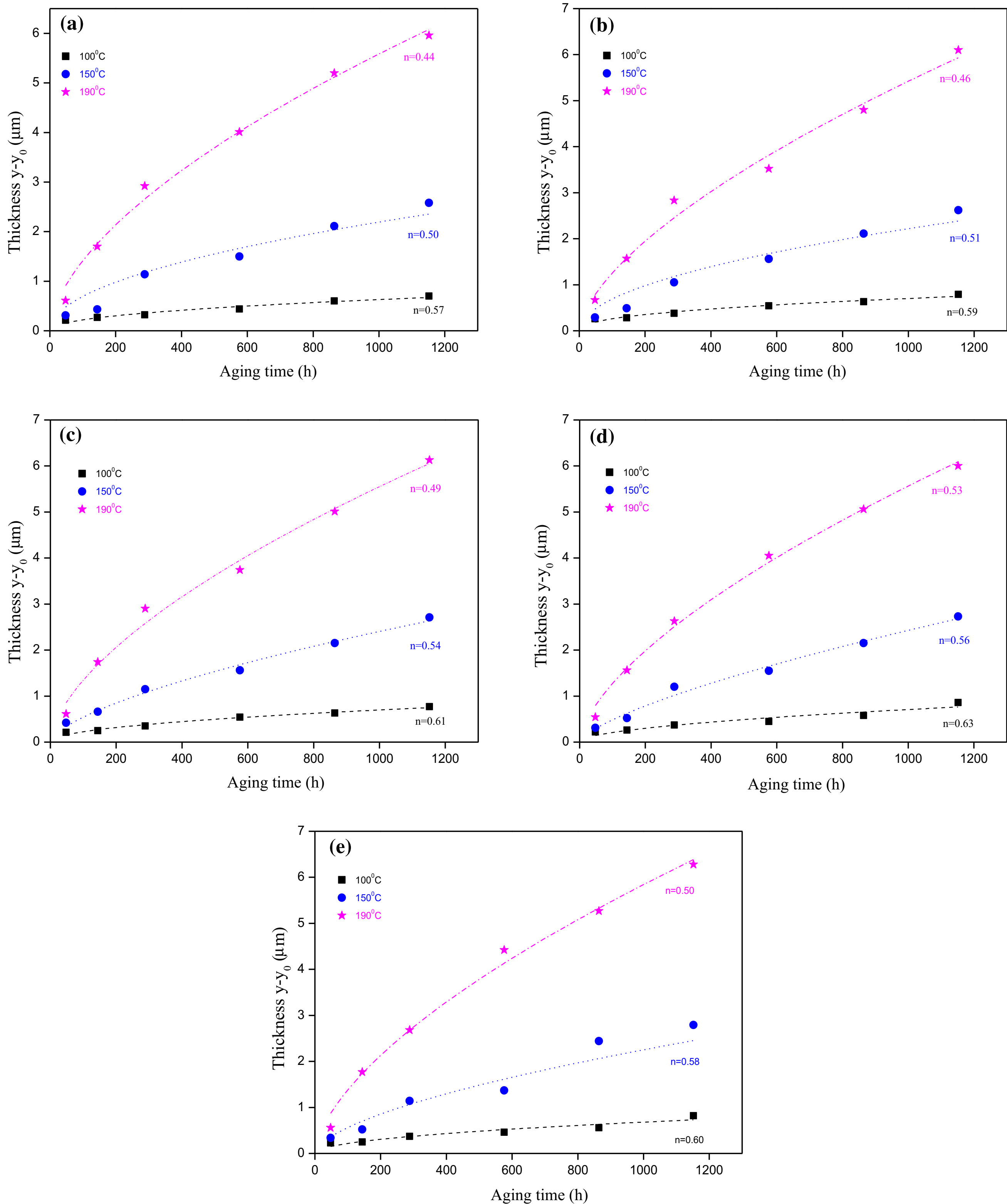

Fig. 13. Thickness of the Cu_3Sn IMC layer versus ageing time for SAC0307-*x*Mn solder joints with different Mn nanoparticle proportions: (a) $x = 0$ wt.%, (b) $x = 0.02$ wt.%, (c) $x = 0.05$ wt.%, (d) $x = 0.1$ wt.%, and (e) $x = 0.15$ wt.%.

the Cu_6Sn_5 phase and $MnSn_2$ phase and that particle B consists of the Ag_3Sn phase and $MnSn_2$ phase. These results are consistent with those of Anderson et al.,[25] who reported that a circular-type $MnSn_2$ phase was present in the Sn-3.5Ag-0.95Cu-0.1Mn solder matrix.

In fact, at the beginning of IMC formation, some Ag_3Sn and Cu_6Sn_5 grains precipitate along the grain boundaries of the Cu_6Sn_5 phase IMC and affect the IMC growth at the solder joint interface. Additionally, based on the classical heterogeneous nucleation theory,[26–28] when Mn nanoparticles are added to the SAC0307 solder, Mn nanoparticles are finely dispersed in the molten solder and are often the preferred sites for Ag_3Sn and Cu_6Sn_5 nucleation, which is consistent with the results of Lin et al.[19] This process will increase the nucleation rate and refine the Ag_3Sn and Cu_6Sn_5 grains, thereby preventing the sequential grain size increase in the IMC phase and promoting the precipitation of refined grains in the channels among the Cu_6Sn_5 layers during the reflow soldering process. In addition, based on the adsorption theory of Mn nanoparticles,[29,30] if the adsorption of Mn nanoparticles increases, the surface energy of Ag_3Sn and Cu_6Sn_5 grains decreases, and the Ag_3Sn and Cu_6Sn_5 grains become smaller during the reflow soldering process. The existence of Ag_3Sn ($MnSn_2$) and Cu_6Sn_5 ($MnSn_2$) particles at the Cu_6Sn_5 grain boundary effectively obstructs the diffusion of Sn and Cu atoms via the IMC layer, as shown in Fig. 10e, f and h, i. This process leads to the inhibition of IMC growth. The grain boundary pinning mechanism could be used to explain why the addition of small quantities of Mn nanoparticles to SAC0307 solder decreases the growth rate of the IMC.

Table II. Relationship between the Mn nanoparticle proportion and the average growth exponents of the Cu_6Sn_5 and Cu_3Sn layers in solder joints

Mn nanoparticle proportion (wt.%)	Average growth exponent	
	Cu_6Sn_5	Cu_3Sn
0	0.57	0.50
0.02	0.59	0.52
0.05	0.60	0.55
0.1	0.61	0.57
0.15	0.58	0.56

For the Cu_6Sn_5 layer, as the Mn nanoparticle proportion increases, the adsorption of Mn nanoparticles by Ag_3Sn and Cu_6Sn_5 crystals increases, and the surface energy of Ag_3Sn and Cu_6Sn_5 grains decreases. This process will increase the number of Ag_3Sn and Cu_6Sn_5 grains per unit volume during the reflow process. Therefore, the number of grains precipitated at the Cu_6Sn_5 grain boundary increases, thereby reducing the growth rate of Cu_6Sn_5 and inhibiting the Cu_6Sn_5 layer growth. When the Mn nanoparticle proportion is 0.1 wt.%, the number of Ag_3Sn and Cu_6Sn_5 grains per unit volume almost reaches a maximum, which leads to the precipitation of a large number of grains at the Cu_6Sn_5 grain boundary, as shown in Fig. 10e, h. Hence, the effect of obstructing the grain boundary diffusion of Cu and Sn atoms via the IMC layer is the most prominent, and the growth rate of the Cu_6Sn_5 layer is minimal for the Mn nanoparticle proportion of 0.1 wt.%. Moreover, when the Mn nanoparticle content increases to 0.15 wt.%, some

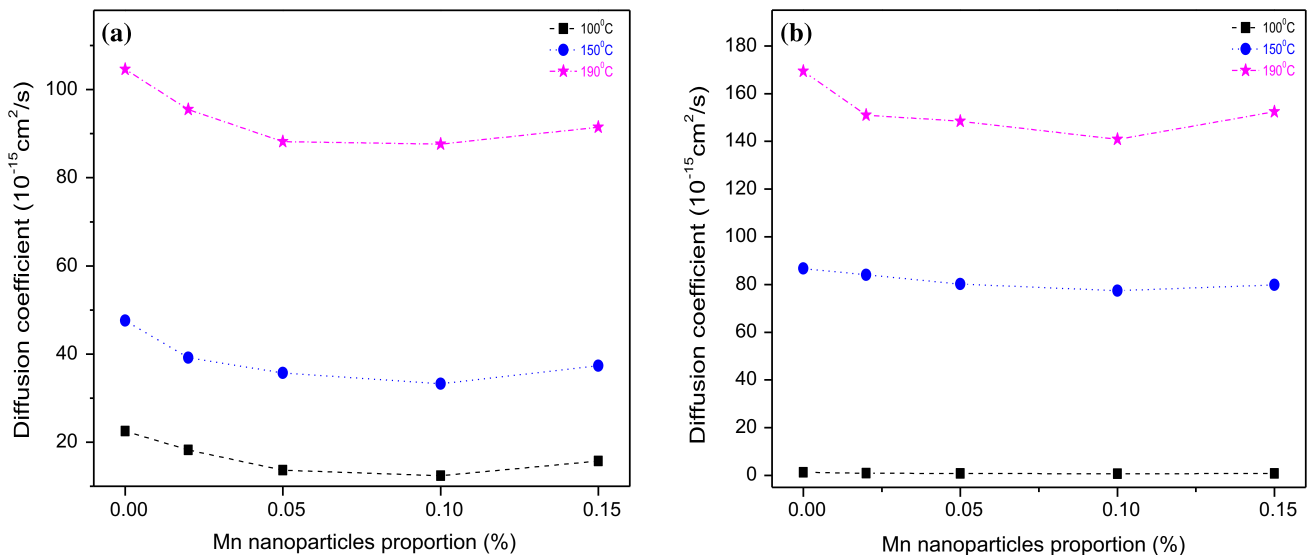

Fig. 14. Diffusion coefficients versus Mn nanoparticle proportion at different ageing temperatures (10^{-15} cm^2/s): (a) Cu_6Sn_5 layer and (b) Cu_3Sn layer.

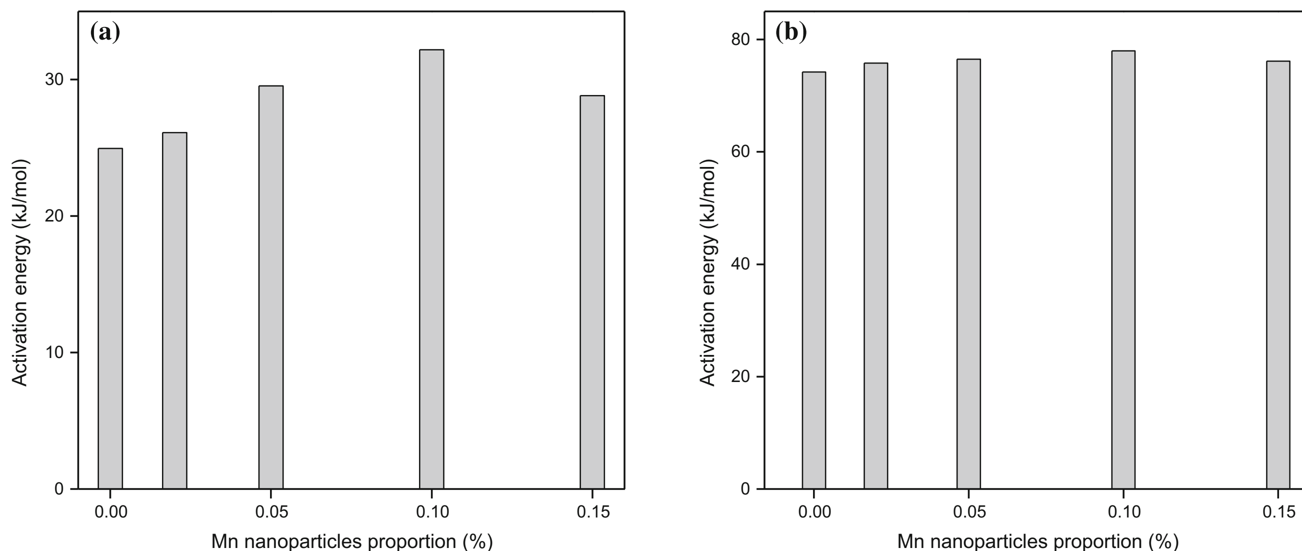

Fig. 15. Relationship between the activation energy and the proportion of Mn nanoparticles: (a) Cu_6Sn_5 layer and (b) Cu_3Sn layer.

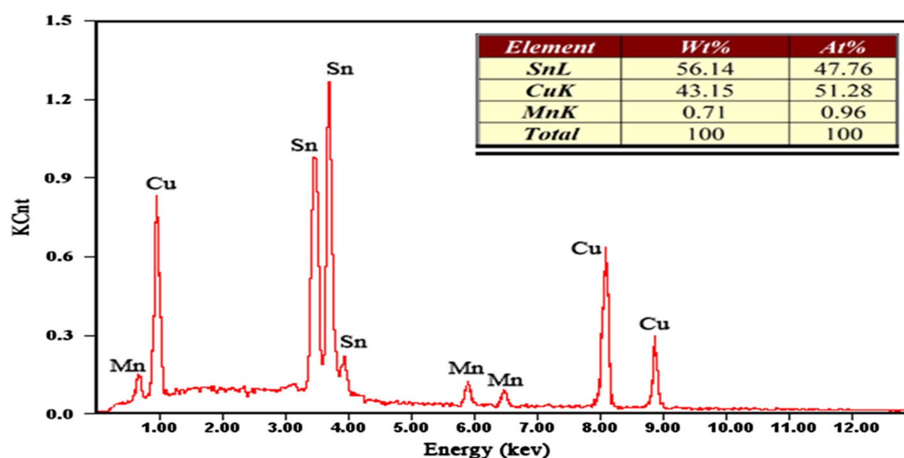

Fig. 16. EPMA analysis of particle A in Fig. 10h.

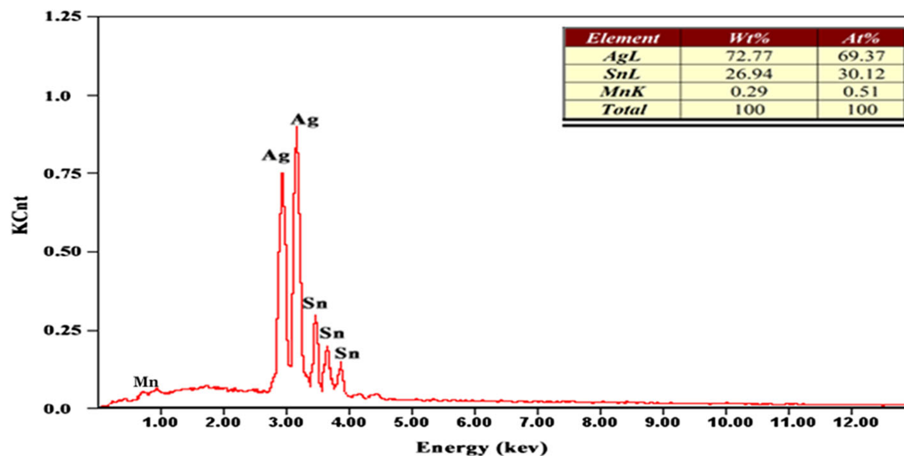

Fig. 17. EPMA analysis of particle B in Fig. 10h.

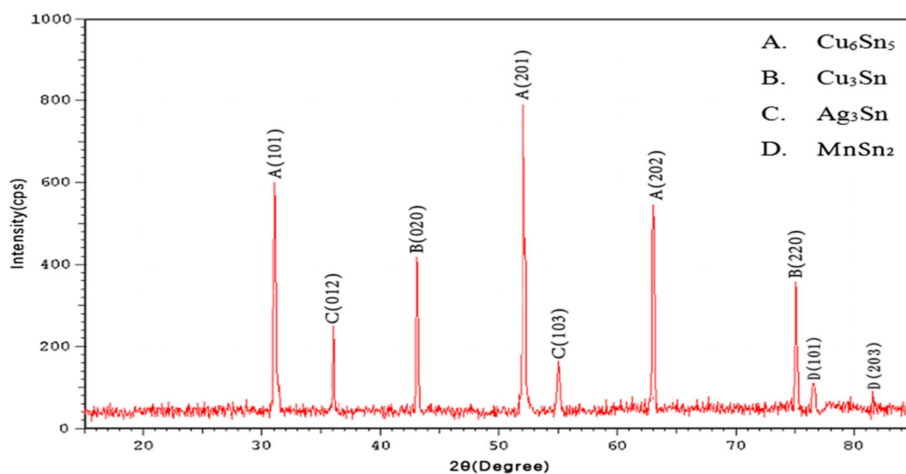

Fig. 18. XRD patterns recorded from the top view of the IMC layer in the SAC0307-0.1Mn solder joints aged at 190°C for 1152 h.

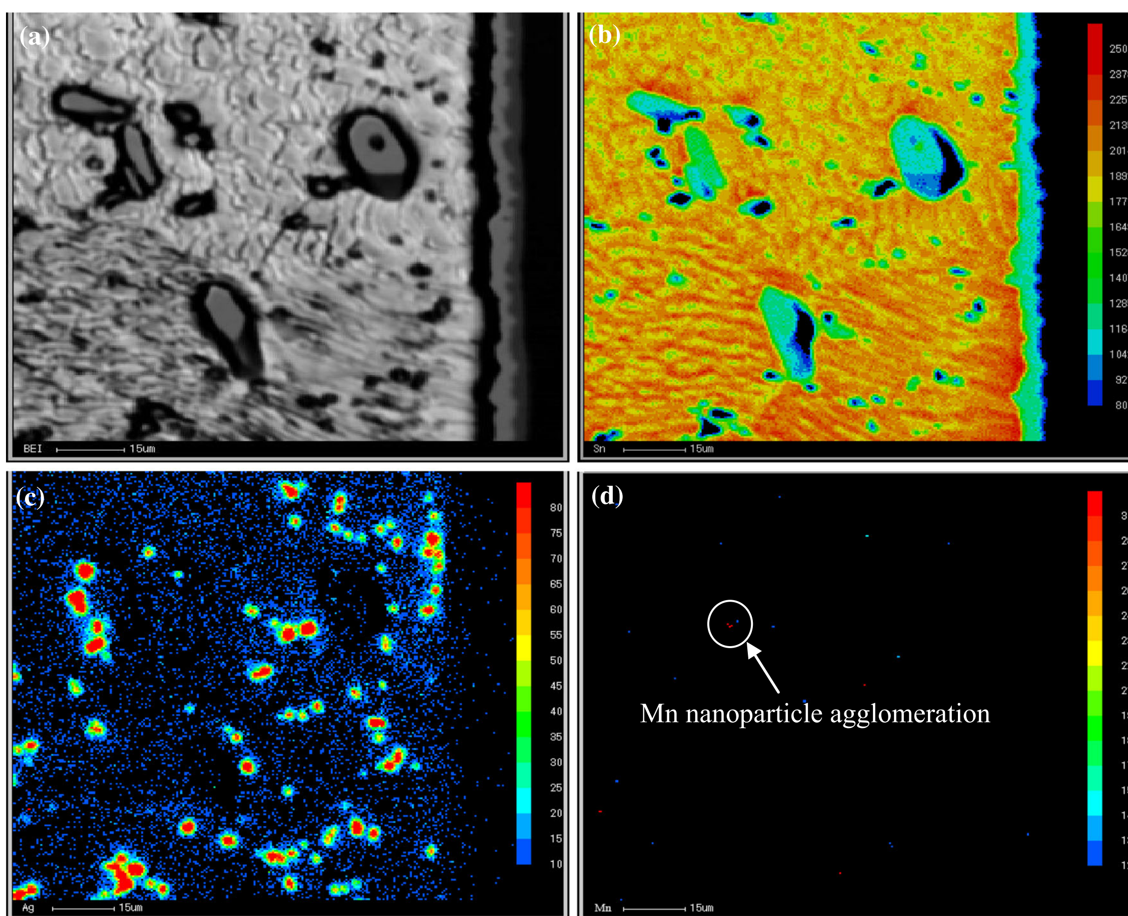

Fig. 19. EPMA mapping images of the SAC0307-0.15 Mn/Cu solder joint aged at 190°C for 864 h: (a) SEM view, (b) Sn mapping, (c) Ag mapping, and (d) Mn mapping.

Mn nanoparticles might be more likely to agglomerate with other Mn nanoparticles. Figure 19 presents the EPMA mapping images of the SAC0307-0.15 Mn/Cu solder joint aged at 190°C for 864 h. The EPMA maps show some Mn nanoparticle agglomeration in the SAC0307-0.15 Mn solder matrix. This agglomeration decreases the number of nucleation sites and inhibits grain refinement. Thus, the number of grains per unit volume precipitated at the Cu_6Sn_5 grain boundary decreases, as

shown in Fig. 10i, and leads to a slight increase in the growth rate of Cu_6Sn_5.

For the Cu_3Sn layer, at a low ageing temperature of 100°C, the growth rate of the Cu_3Sn layer remains almost unaffected by Mn nanoparticle addition because the growth rate is notably low, and the availability of Sn is not a key factor in the formation of Cu_3Sn. This finding agrees with the results observed by Deng et al.[31] One major process that contributes to the Cu_3Sn layer growth is Cu atoms from the Cu substrate arriving at the Cu_3Sn/Cu_6Sn_5 interface by interstitial diffusion and reacting with the Cu_6Sn_5 phase to form the Cu_3Sn phase by consuming the Cu_6Sn_5 phase. At a high ageing temperature of 190°C, the effect of the Mn nanoparticles on Cu_3Sn layer growth exhibits the same trend as that for the Cu_6Sn_5 layer. This trend is due to the Sn diffusion mechanism being predominant at high ageing temperatures, and the major process that contributes to the Cu_3Sn layer growth is the diffusion of Sn atoms from the solder matrix through the Cu_6Sn_5 and Cu_3Sn layers and reaching the Cu_3Sn/Cu interface to react with Cu and form the Cu_3Sn phase. Because of the addition of Mn nanoparticles, an increase in the quantity of small particles precipitated and pinned along the grain boundary of the Cu_6Sn_5 layer limits the availability of Sn atoms arriving at the Cu_3Sn/Cu interface for the formation of a Cu_3Sn layer. Moreover, considering the Cu_3Sn layer that grew at the expense of the Cu_6Sn_5 phase, the growth rate of the Cu_3Sn layer considerably increases, becoming even higher than that of the Cu_6Sn_5 layer at a higher ageing temperature.

CONCLUSIONS

In this study, the morphological evolution and growth kinetics of interfacial Cu_6Sn_5 and Cu_3Sn IMC layers in low-Ag SAC0307-*x*Mn/Cu solder joints during isothermal ageing were studied. The main conclusions are as follows:

1. At low ageing temperatures, the Cu_6Sn_5 layer plays a dominant role in the growth of the total IMC layer, whereas the Cu_3Sn layer substantially contributes to the total IMC layer at high ageing temperatures. Both the Cu_6Sn_5 and Cu_3Sn layers in the Mn-containing solder joints are thinner than those in the Mn-free solder joints under identical ageing conditions. Kirkendall voids form at the Cu/Cu_3Sn interface and in the Cu_3Sn IMC layer at high ageing temperatures.
2. The growth exponent value of the Cu_6Sn_5 layer is near 0.5 at high ageing temperatures but substantially deviates from 0.5 at low ageing temperatures. This finding indicates that Cu_6Sn_5 layer growth is mainly dominated by a diffusion-controlled mechanism at high ageing temperatures and a combination of diffusion-controlled and interface reaction-controlled mechanisms at low ageing temperatures. The Cu_3Sn layer grows faster than the Cu_6Sn_5 layer at high ageing temperatures and slower at low ageing temperatures.
3. The solder with approximately 0.1 wt.% Mn nanoparticles added exhibits the highest activation energies and the lowest growth rates for both the Cu_6Sn_5 and Cu_3Sn layers. The addition of Mn nanoparticles strongly affects Cu_6Sn_5 layer growth but weakly impacts Cu_3Sn layer growth, particularly at low ageing temperatures.
4. The effect of Mn nanoparticle addition on Cu_6Sn_5 layer growth can be explained by a grain boundary pinning mechanism. The small particles that precipitate and become pinned along the grain boundaries obstruct the Sn and Cu atoms from diffusing through the grain boundaries, thereby suppressing the formation of the IMC in the solder joint.

ACKNOWLEDGEMENTS

The authors acknowledge the support of the Project of Guangdong Province Universities and Colleges Pearl River Scholar Funded Scheme, China (Grant No. 2016), the Project of Guangdong Province Support Plans for Top-notch Youth Talents, China (Grant No. 2016TQ03N704), the Pearl River S&T Nova Program of Guangzhou, China (Grant No. 201610010157), and the Outstanding Young Teacher Project of Guangdong Province Universities and Colleges, China (Grant No. YQ2015093).

REFERENCES

1. Y. Liu, F. Sun, Y. Liu, and X. Li, *J. Mater. Sci. Mater. Electron.* 25, 2627 (2014).
2. A.A. El-Daly, A.E. Hammad, G.S. Al-Ganainy, and M. Ragab, *Mater. Sci. Eng. A* 608, 130 (2014).
3. D.X. Luo, S.B. Xue, and S. Liu, *J. Mater. Sci. Mater. Electron.* 25, 5195 (2014).
4. M. Yang, Y.H. Ko, J. Bang, T.S. Kim, C.W. Lee, and M. Li, *Mater. Charact.* 124, 250 (2017).
5. N. Mookam and K. Kanlayasiri, *J. Mater. Sci. Technol.* 28, 53 (2012).
6. K. Kanlayasiri, M. Mongkolwongrojn, and T. Ariga, *J. Alloys Compd.* 485, 225 (2009).
7. N. Mookam and K. Kanlayasiri, *J. Alloys Compd.* 509, 6276 (2011).
8. X. Yan, K. Xu, J. Wang, X. Wei, and W. Wang, *Solder Surf. Mt. Tech.* 28, 215 (2016).
9. F. Cheng, F. Gao, J. Zhang, W. Jin, and X. Xiao, *J. Electron. Mater.* 46, 3424 (2011).
10. L.C. Tsao, S.Y. Cheng, C.W. Chen, and T.Y. Chen, *Mat. Sci. Eng. A* 658, 159 (2016).
11. R.W. Wu, L.C. Tsao, and R.S. Chen, *J. Mater. Sci. Mater. Electron.* 26, 1858 (2015).
12. K. Kanlayasiri and K. Sukpimai, *J. Alloys Compd.* 668, 169 (2016).
13. H. Wang, S. Xue, and J. Wang, *J. Mater. Sci. Mater. Electron.* 28, 8246 (2017).
14. J. Wu, S. Xue, J. Wang, J. Wang, and S. Liu, *J. Mater. Sci. Mater. Electron.* 28, 10230 (2017).

15. Y. Gu, X. Zhao, Y. Li, Y. Liu, Y. Wang, and Z. Li, *J. Alloys Compd.* 627, 39 (2015).
16. Y.M. Leong and A.S.M.A. Haseeb, *Materials* 9, 522 (2016).
17. D.A. Shnawah, S.B.M. Said, M.F.M. Sabri, I.A. Badruddin, and F.X. Che, *J. Electron. Mater.* 41, 2631 (2012).
18. W. Liu, N.C. Lee, A. Porras, M. Ding, A. Gallagher, A. Huang, S. Chen, and J. C. Lee, *Electronic Components and Technology Conference (2009)*, pp. 994–1007.
19. L.W. Lin, J.M. Song, Y.S. Lai, Y.T. Chiu, N.C. Lee, and J.Y. Uan, *Microelectron. Reliab.* 49, 235 (2009).
20. Y. Tang, S.M. Luo, K.Q. Wang, and G.Y. Li, *J. Alloys Compd.* 684, 299 (2016).
21. G.Y. Li, X.D. Bi, Q. Chen, and X.Q. Shi, *J. Electron. Mater.* 40, 165 (2011).
22. W.L. Chiu, C.M. Liu, Y.S. Haung, and C. Chen, *Mater. Lett.* 164, 5 (2016).
23. C.E. Ho, T.T. Kuo, C.C. Wang, and W.H. Wu, *Electron. Mater. Lett.* 8, 495 (2012).
24. L. Zhang and L.L. Gao, *J. Alloys Compd.* 635, 55 (2015).
25. I.E. Anderson, J.W. Walleser, J.L. Harringa, F. Laabs, and A. Kracher, *J. Electron. Mater.* 38, 2770 (2009).
26. C.C. Pan, C.H. Yu, and K.L. Lin, *Appl. Phys. Lett.* 93, 061912 (2008).
27. D.A. Porter and K.E. Easterling, *Phase Transformations in Metals and Alloys* (London: Chapman & Hall, 1981).
28. R.E. Reed-Hill, *Physical Metallurgy Principles* (Boston: PWS, 1972).
29. L.C. Tsao, *J. Alloys Compd.* 509, 2326 (2011).
30. L.C. Tsao, *J. Alloys Compd.* 509, 8441 (2011).
31. X. Deng, G. Piotrowski, J.J. Williams, and N. Chawla, *J. Electron. Mater.* 32, 1403 (2013).